Earth and Planetary Science Letters 275 (2008) 93–101

Contents lists available at ScienceDirect

Earth and Planetary Science Letters

journal homepage: www.elsevier.com/locate/epsl

Andean growth and the deceleration of South American subduction: Time evolution of a coupled orogen-subduction system

Brendan J. Meade [a,*], Clinton P. Conrad [b]

[a] Department of Earth and Planetary Sciences, Harvard University, 20 Oxford Street Cambridge, MA 02138, United States
[b] Department of Geology and Geophysics, University of Hawaii at Manoa, 1680 East-West Road, Honolulu, HI 96822, United States

ARTICLE INFO

Article history:
Received 28 May 2008
Received in revised form 4 August 2008
Accepted 6 August 2008
Available online 17 September 2008

Editor: R.D. van der Hilst

Keywords
tectonic plate motions
subduction
orogen development
plate boundary zones
Nazca Plate
Andes
erosion
climate

ABSTRACT

Present-day orography at the Andean margin is a result of isostasy, tectonic accretion, and erosional processes. The resulting excess mass of the Andes gives rise to frictional stresses on the seismogenic plate interface that resist the sinking of the subducting slab into the upper mantle. Thus, subduction rates should be sensitive to the time-dependent dynamics of a back-arc orogen, as well as erosional or accretional processes that affect orogen growth. Here we develop a two-dimensional coupled orogen–slab model that allows for the prediction of orogen size and plate motion in response to both tectonic and erosional forcing. We find that the frictional force exerted by the orogen on the subducting slab grows quadratically with orogen width and that the frictional resistance typically balances 10–50% of the slab pull force. The time evolution of the coupled orogen-subduction zone system is largely controlled by the rate of orogen growth, which is controlled by the rate of convergence and the erosivity of the climate state. In the case of the Andean margin, our models show that Miocene aridification leads to reduced erosion, increased orogen growth, greater frictional resistance to subduction, and, ultimately, to a ~50% reduction in the convergence rate between the Nazca and South American plates.

1. Introduction

The highest mountains on Earth are found in orogens at convergent plate margins that are characterized by the great relief (>7 m), active shortening (>20 m/yr), and widespread seismic activity (M_W>8) associated with either shallowly dipping crustal thrust faults (e.g., India–Asia collision zone) or major subduction zone interfaces (e.g., Andean margin). Over the last two decades quantitative models have been developed in an effort to understand how these dynamic boundaries develop in response to variations in tectonic accretion and erosional mass removal rates. Quasi-static two-dimensional analytic models have provided first-order descriptions of the kinematics of mass transport and energy partitioning within an orogen as well as the characteristic scalings that describe the magnitude of the orogenic response to tectonic and erosional forcings (Barr and Dahlen, 1988; Whipple and Meade, 2006; Hilley and Strecker, 2004; Roe et al., 2006). Computational methods have allowed for the direct solution of the equations of motion in an orogenic system including the effects of strong variations in material properties and spatially variable surface processes (e.g., Willett, 1999; Beaumont et al., 2001; Stolar et al., 2007). While all of these models have focused on orogen development in response to external forcing, the potential feedbacks between orogen size and the tectonic convergence rate have been largely neglected.

The premise that the growth of the Andes might give rise to a force that slows the convergence between the Nazca (NAZ) and South American (SAM) plates has been discussed in a few recent papers (Norabuena et al., 1999; Garzione et al., 2006; Iaffaldano et al., 2006; Husson et al., 2008). Both Garzione et al. (2006) and Ghosh et al. (2006) exploited oxygen isotope paleo-thermometers and estimates of the adiabatic lapse rate to estimate the paleo-elevation of carbonate paleosols preserved in the Bolivian Altiplano finding that at least ~2.5–3.5 km of surface uplift occurred between ~10.3 and 6.8±0.4 Ma. This rapid surface uplift has been argued to result from the isostatic adjustment of the crust in response to mass loss at depth due to a Raleigh–Taylor instability, and the foundering of eclogitic lower crust (Garzione et al., 2006; Ghosh et al., 2006; Molnar and Garzione, 2007). Garzione et al. (2006) demonstrated that the resulting topographic gradient from the high Altiplano to the Nazca plate would result in an increase in the compressional force (per unit length) of 0.6×10^{12} N/m and suggested that this additional force may have contributed to the late Miocene deceleration of the NAZ–SAM convergence rate. Iaffaldano et al. (2006) used a thin shell lithosphere model coupled

* Corresponding author.
E-mail addresses: meade@fas.harvard.edu (B.J. Meade), clintc@hawaii.edu (C.P. Conrad).

0012-821X/$ – see front matter © 2008 Elsevier B.V. All rights reserved.
doi:10.1016/j.epsl.2008.08.007

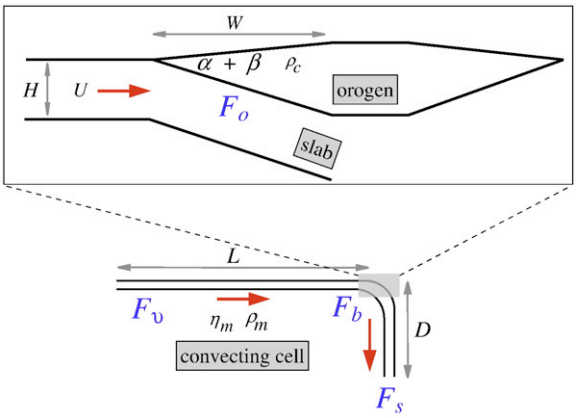

Fig. 1. Illustration of the components of the coupled orogen-subduction system. The boxed area shows the geometry at the orogen-subduction zone interface that corresponds to the upper right hand corner (shaded) of the convecting upper mantle cell in the lower panel. The red arrows indicate the sense of motion, the gray arrows indicate the length extents of the labeled features, and the variables are defined in the text.

to a global mantle circulation model to quantify the magnitude of deceleration that results from the sudden emplacement of the Andes. These models predict a linear decrease in NAZ–SAM convergence (from ~10 to ~7 cm/yr) and a linear increase in Altiplano elevation (from ~1.5 to ~3.8 km) over the last ~10 Ma. Finally, Husson et al. (2008) suggested that westward push from Andean growth could initiate a net westward drift of the entire Pacific basin, but did not examine the time-dependent development of this system.

To better understand the Andean margin in particular and the behavior of an orogen-subduction system in general, we developed a two-dimensional model of a coupled orogen-subduction zone system. The sizes of both the orogen and the subducting slab evolve in a kinematically consistent manner in response to changes in plate convergence rate and the removal of orogenic material by erosional processes. This model allows us to make quantitative predictions for the time evolution of both orogen size and plate convergence rate as a function of the most important factors that describe the system: orogen geometry, plate geometry, mantle viscosity, erosivity of the climate state, isostatic compensation, and the frictional behavior of the subduction zone interface. Because the force balance evolves over orogen evolution time scales (1–10 Ma, Whipple and Meade, 2006), plate motions can change rapidly in response to orogenic growth modulated by changes in climate state.

2. Force balance in a coupled orogen-subduction system

To understand the behavior of a coupled orogen-subduction system, we consider a simple two-dimensional model where an orogenic wedge sits atop the oceanic lithosphere in the upper right hand corner of a convecting upper mantle cell (Fig. 1). Previously, the effect of the orogen has been neglected, and the motion of the subducting plate has been determined from a force balance between the slab pull driving force F_s, resisting forces associated with viscous drag from upper mantle deformation F_v, and bending of the subducting plate F_b (Forsyth and Uyeda, 1975; Conrad and Hager, 1999; Buffett, 2006). To these resisting forces, we add the force exerted by the orogen on the subducting plate, F_o, which we define below. Thus the complete force balance gives,

$$F_s = F_v + F_b + F_o. \quad (1)$$

The forces F_s, F_v, and F_b have been defined previously. The driving force exerted by negative buoyancy of the slab sinking into the upper mantle is, $F_s = \Delta\rho g H D$, where $\Delta\rho$ is the average difference between slab and mantle densities, g is the acceleration of gravity, H is the thickness of the subducting oceanic lithosphere, and D is the depth to which the subducting slab acts as a stress guide (Elsasser, 1969; Forsyth and Uyeda, 1975; Conrad and Hager, 1999), which typically consists of the upper mantle portion of the slab (Conrad and Lithgow-Bertelloni, 2002; Conrad et al., 2004). The viscous drag force, $F_v = \eta_m UL/D$, results from upper mantle shear generated by the motion of a subducting plate of length L moving across the upper mantle of viscosity η_m with speed U (Conrad and Hager, 1999). The resistance to plate bending at the subduction zone can be expressed as a force, $F_b = 2\eta_b U (H/R)^3 /3$, where H is the plate thickness (assumed equal to the value used to define F_s), R is the radius of curvature of bending, and η_b is the effective viscosity of the bending lithosphere (Buffett, 2006).

The total resistive shear force exerted by the orogen on the slab is given by the integral of the normal stress, σ_n, exerted by the orogen's weight on the plate bounding fault, multiplied by the effective coefficient of friction, μ. Here we treat the orogen as a brittle frictional wedge (Chapple, 1978; Davis et al., 1983; Dahlen, 1984; Dahlen and Suppe, 1988) with cross-sectional area, A, surface slope, α, and basal dip, β. Orogen size is controlled by the balance between tectonic accretion and erosional mass removal (Barr and Dahlen, 1988; Willett, 1999; Whipple and Meade, 2004). Material accretes into the orogen at a rate that is proportional to the convergence rate, U, multiplied by the thickness of the accretionary aperture, h, which is typically smaller than the thickness of the incoming lithosphere, H. In general, orogens, such as Taiwan (Suppe, 1980) and the Andes (e.g., Isacks, 1988), accrete material from the landward side of the subduction zone interface though there are exceptions such as the Himalayan range front at the India–Asia collision zone (e.g., Lave and Avouac, 2001). For self-similar two-sided orogens (e.g., Whipple and Meade, 2004), both sides grow in width proportionally so that accretion on the non-subducting side causes growth of the entire orogen. For the case of the Andes where the Eastern and Western Cordillera are separated by the flat Altiplano, material accreted along the eastern margin may contribute to the surface uplift of the western margin through the transport of material along deep low angle thrust faults (McQuarrie, 2002), or ductile flow (Lamb and Hoke, 1997) in the lower crust underlying the central plateau. Thus, accretion on either side of the orogen contributes to an increase in overall cross-sectional area, and thus the width, W, of the orogenic wedge that is in contact with, and frictionally coupled to, the subduction zone interface (1). The width of the frictional (seismogenic) subduction zone interface does not grow but is limited to the region above the brittle–ductile transition depth, D_t so that the maximum width is $W = D_t/\tan(\beta)$ which is typically in excess of 200 km for shallowly dipping ($\beta < 10°$) subduction zones. Further, we assume that the elevation of the Altiplano is coupled to, and can never be greater than, its active eastern and western margins.

For a wedge-shaped orogen where the normal stress at the subduction zone-orogen interface is lithostatic, the shear stress grows geometrically with the width of the orogen, $F_o = \mu p_c g W^2(\tan\alpha + \tan\beta)$. In two-dimensions, or per unit trench length, the width of an orogen in contact with a slab is related to the cross-sectional area of the orogenic wedge as $W = \sqrt{2A\tan\alpha(\rho_m - \rho_c)/\rho_c \tan\alpha}$. Here the shear stress exerted by the orogen on the slab grows quadratically with width. This contrasts with the linear force-width scaling assumed in models that neglect the wedge-shaped geometry of the orogen and subduction zone interface by assuming that a thin shell representation of the lithosphere accurately predicts stresses exerted by the orogen on the top of the convecting mantle cell (Iaffaldano et al., 2006). Combining our expressions for F_s, F_v, F_b and now F_o into the force balance (Eq. (1)), we obtain an expression for the slab-orogen interface width at steady state,

$$W_s = \sqrt{\frac{\Delta\rho g H D - 2\eta_b U (H/R)^3/3 - \eta_m UL/D}{\mu\rho_c g(\tan\alpha + \tan\beta)}}. \quad (2)$$

The rate of subduction convergence, which is equivalent to the subducting plate speed U relative to the stationary wedge, for a given geometric configuration, is,

$$U = \frac{\Delta\rho g H D - (\mu\rho_c g(\tan\alpha + \tan\beta))W^2}{2\eta_b (H/R)^3/3 + \eta_m L/D}. \quad (3)$$

Note that these relationships technically apply only for the quasi-static case where the orogen is at mass flux steady state because we have ignored the inertial terms in the force balance (Eq. (1)). However, these terms are unimportant for low Reynold's number systems such as the mantle. Therefore, we can assume that geological rates of change of W_s or U are so slow that Eqs. (2) and (3) apply even when the orogen is growing or shrinking. As we shall see, the magnitude of the resisting force F_o associated with orogens such as the Andes can be a significant fraction of the slab pull force F_s. Thus, F_o can significantly slow the subducting plate speed U by diminishing the numerator of Eq. (3).

3. Time evolution of a coupled orogen-subduction system

The temporal evolution of the force exerted by the orogen on the subducting plate is proportional to the mass of the orogen above the frictional interface. Orogen size evolves in response to the difference between the rate at which material is accreted into an orogen by tectonic processes and the rate at which it is removed by erosional processes. The rate of mass accretion per unit width is equal to the convergence rate multiplied by the thickness of the accreting layer h that is incorporated into the orogen. Based on Hack's law describing the shape of drainage basins (Hack, 1957), characteristic hydraulic geometry, empirically constrained relationships for erosion rate as a function of local channel slope, and the assumption that most relief in an orogen is generated by fluvial processes, Whipple and Meade (2004) derived an orogen-scale erosion law for the mean erosion rate of an orogen as $\varepsilon_o = CW^a \tan\alpha^b$, where C is the erosivity due to the combination of climate state and effective rock strength. Combining the orogen scale erosion law with the assumption of self-similar wedge geometry, the temporal evolution of the cross-sectional area A is given by,

$$\frac{dA}{dt} = Uh - KA^p \quad (4)$$

where h is the thickness of the accreting layer (Fig. 1) and p describes how erosion rates grow with orogen width due to the orogen-scale erosion law described above (Whipple and Meade, 2006). Additional sources of mass input including tectonic underplating (e.g., Dahlen and Barr, 1989) and the recycling of eroded material (e.g., Whipple and Meade, 2004) are neglected here. Barr and Dahlen (1989) assumed $p = 1/2$ (i.e., mean erosion rate is not a function of orogen width) while Whipple and Meade (2006) showed that the combination of any channel erosion law that is a monotonically increasing function of local slope and a drainage network geometry scaling that follows Hack's law (Hack, 1957) gives $0.7 \le p \le 1.2$. Here we use an intermediate value, $p = 1$, throughout. The coefficient K in Eq. (4) is the effective erosional efficiency (Whipple and Meade, 2006) and is proportional to the erosion coefficient derived from stream power and shear stress dependent erosion laws, K'. These studies model channel incision rates, ε, as a function of erosivity of climate/rock resistance K', drainage area A_D (which serves as a proxy for discharge Q), and slope S, such that $\varepsilon = K' A_D^m S^n$, (where m and n are the discharge and slope exponents respectively) and found $K' = 10^{-5}$–10^{-7} (e.g., Seidl and Dietrich, 1992; Whipple and Tucker, 1999; Kirby and Whipple, 2001; Wobus et al., 2003). In general, the discharge Q is given by the integral of the precipitation (e.g., mean annual) distribution over the drainage area, so for the case of spatially uniform precipitation, P_0, the discharge is then $Q = P_0 k_a x^{b_H}$ where x is the downstream distance, $k_a \sim 6$, and $b_H \sim 1.8$ are the Hack coefficient and exponent, respectively (Hack, 1957). Using this explicit representation of the precipitation rate, an orogen-scale erosion law, and assuming isostatic compensation of the orogen, the erosional efficiency is,

$$K = \frac{K'(P_0 k_a)^m (\rho_m - \rho_c)}{\rho_m}\left(1 - \frac{hm}{n}\right)^n. \quad (5)$$

In general K has been parameterized as a variable whose dimensions depend on other empirically derived scaling relationships such as Hacks law, and the value of m. Both field and theoretical studies have constrained the ratio of these exponents to $m/n = 0.35$–0.60 (e.g., Whipple and Tucker, 1999; Wobus et al., 2003). For the case of detachment-limited incision, $n = 2$ and $m = 1$ so that the incision rate scales linearly with precipitation rate, and Eq. (5)) reduces to $K = (0.33$–$10^{-3}) \times K'$ where the quantity $(P_0 k_a)$ is treated as dimensionless and K has dimensions of yr^{-1}. Interestingly, the effective erosion coefficient scales linearly with the mean annual precipitation rate only for $m = 1$ and the smaller values of the discharge (or more commonly, drainage area) exponent, which predicts a damped response to precipitation forcing. The relationships for steady state orogen width and convergence rate (Eqs. (2), (3)) can be written in terms of the erosivity by applying $dA/dt = 0$ to Eq. (4) to get $U = KW^2\rho_c/(2h(\rho_m - \rho_c)\tan\alpha)$.

The second component of the model that evolves geometrically in time is the depth of the subducting slab, D. For the models presented here, the slab depth D increases monotonically and at a rate proportional to the convergence rate,

$$\frac{dF_s}{dt} = \Delta\rho g H U \sin\delta \quad (6)$$

where δ is the mean dip of the slab. For the examples that follow, $\delta = 90°$ so that we can make clear the behavior of the system with the strongest possible subduction driving force. We also limit the slab to the upper mantle (thus $D \le 670$ km) because lower mantle slab weight is thought to be supported by viscous stresses, rather than guiding stresses within the slab that generate slab pull (Conrad and Lithgow-Bertelloni, 2002; Conrad et al., 2004). By substituting Eq. (3) into Eqs. (4) and (6) we have a closed system of two coupled ordinary differential equations that describes the time evolution of orogen size and convergence rate. To understand the behavior and sensitivities of this system, we now consider several forward models. In the sections that follow we will apply this model to the Andes and the Nazca–South America plate boundary and so we utilize a parameter range appropriate for that locale for these examples. A discussion of applicable values of K_0 for the Andes is presented in the next section though characteristic values are used in the examples that follow. We consider four hypothetical cases of how this system evolves in time: 1) uniform erosivity (constant K), 2) uniform erosivity with delayed orogen initiation, 3) a step-like change in erosivity, and 4) continually varying erosivity where no steady state is reached. In all of these cases we start with the initial condition that there is no orogen. For cases 1) and 2) we show the development as a function of three initial slab depths $D_0 = (200, 400, 670)$ km while for cases 3) and 4) $D_0 = 670$ km. In all models, $L = 3000$ km to approximate the distance between the East Pacific Rise and the South American Trench, $\alpha = 2°$, $\beta = 8°$ (Vietor and Oncken, 2005), $\rho_m = 3300$ kg/m^3, $\rho_c = 2700$ kg/m^3, $\eta_m = 5 \times 10^{20}$ Pa·s (Mitrovica, 1996), $\mu = 0.4$ (e.g., Bird and Kong, 1994), and the effective plate bending viscosity is $\eta_b = 300\ \eta_m$ Pa·s (Conrad and Hager, 1999; Buffett, 2006) with $R = 200$ km, $H = 2\sqrt{\kappa T}$ where κ is the thermal diffusivity of basalt and $T = 40$ Ma is the age of the oceanic plate at the subduction zone.

With an erosion rate that is constant in time, $K = 10^{-7}$ yr^{-1}, and the initial condition of no orogen, both the orogen width and the plate convergence rate evolve to steady state values in ~10 Ma (Fig. 2a, b). This time scale is weakly sensitive to the initial slab depth with the

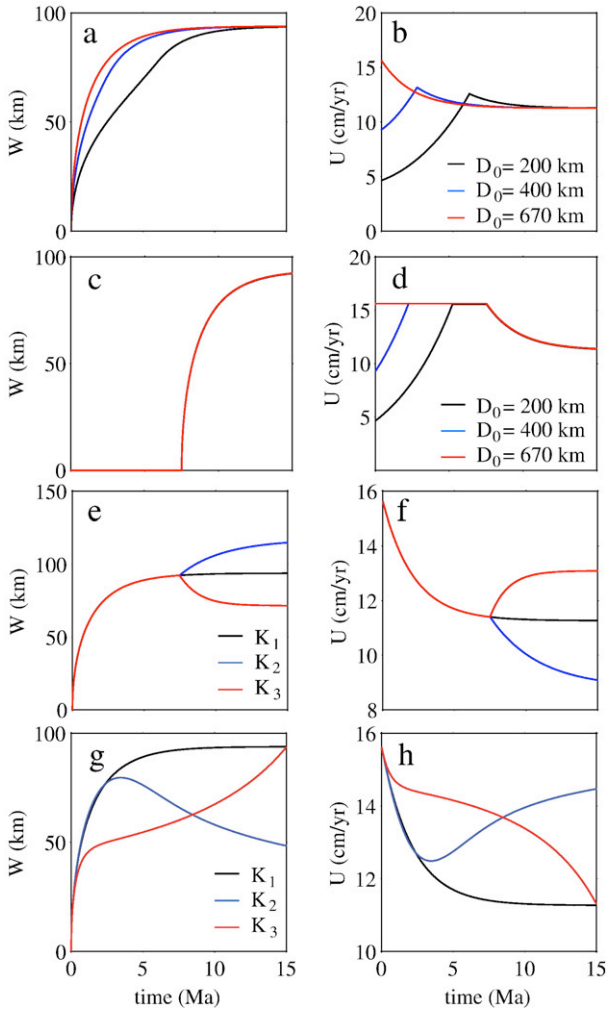

Fig. 2. Time histories for orogen width (left-hand column) and plate convergence rates (right hand column). The upper two panels (a, b) show the evolution when K_0 is constant in time and equal to 10^{-7} yr^{-1}. The black, blue, and red lines represent the initial depths (D_0=200, 400, and 670 km respectively) of the slab at the time that the orogen starts to grow. Note that the convergence rate approaches a steady state value from both faster and slower rates depending on D_0. Panels c and d show time histories for orogen width and plate convergence rates with a delay in the onset of orogen growth, again for constant $K_0=10^{-7}$ yr^{-1} and varying initial depths D_0 as in (a, b). In this case, orogen development is initiated at 7.5 Ma in each model run. Note that the absence of an orogen allows the plate convergence rate to increase with no additional resistance until orogen growth is initiated at 7.5 Ma. Panels e and f show time histories for orogen width and plate convergence rates with a sudden change in the erosivity of climate at 7.5 Ma. Initially K_0 is constant in time and equal to 10^{-7}. At 7.5 Ma the erosivity doubles (red), halves (blue), and remains constant (black). Panels g, h show time histories for orogen width and plate convergence rates with time-variable erosivity. The three cases are: 1) K_1, constant, $K=10^{-6}$, 2) K_2, linear increase from $K=5\times10^{-7}$ to $K=5\times10^{-6}$, and 3) K_3, linear decrease from $K=5\times10^{-6}$ to $K=5\times10^{-7}$.

shallowest (200 km) initial slab depth model taking the longest time to approach steady state due to the relatively low initial value of the slab pull force. While the time scales for the evolution to steady state do not vary substantially as a function of D_0, the primary direction from which these models approach the steady state convergence rate is relatively distinct (Fig. 2b). If orogen growth initiates when the slab is already at a depth of 670 km, then the growing orogen exerts a shear traction that decelerates the plate convergence rate. In contrast, the D_0=200 and 400 km initial conditions give rise to an initial increase in convergence rate due to the fact that the slab pull force initially increases faster than does the resisting shear stress of the nascent orogen. A 7.5 Ma, delay in the onset of orogen growth allows the D_0=200 and 400 km slabs to reach the 670 km transition zone before orogen growth is initialized. These slabs achieve a temporarily steady convergence rate after ~5 Ma (Fig. 2c, d). Note that the last 7.5 Ma of all three models shown in (Fig. 2c, d) are identical to the D_0=670 km case in Fig. 2a, b. For a basal dip of β=8°, the maximum depth of the assumed orogen–slab interface is ~20 km and so is within the regime of observed frictional deformation (Pritchard et al., 2006).

If the mechanically coherent slab extends to a depth of 670 km throughout the period of observation, both orogen size and plate convergence rate may evolve non-monotonically as a result of changes in the erosivity of the climate state. Consider the case where $K=10^{-7}$ yr^{-1} for the first 7.5 Ma of each model run then either doubles (to $K=2\times10^{-7}$ yr^{-1}), halves (to $K=0.5\times10^{-7}$ yr^{-1}), or remains constant (Fig. 2e, f). In all cases the orogen initially grows and slows the plate convergence rate. When the erosivity is increased at 7.5 Ma, the orogen shrinks because orogen mass is removed more rapidly for a given orogen width. This results in the development of both a smaller orogen and an increase in the plate convergence rate. The converse occurs when the erosivity is reduced by a factor of two at 7.5 Ma. In this case the orogen grows and widens until orogen material is removed rapidly enough to reach steady state. As this occurs, the width of the orogen increases by ~25% and the convergence rate drops by ~40%. Abrupt changes in erosivity can result from changes in global or local climate state. In fact, changes to the local climate state may result from orogen growth itself via enhancement of orographic precipitation (Roe and Baker, 2006). An increase in orographic precipitation may have the effect of increasing

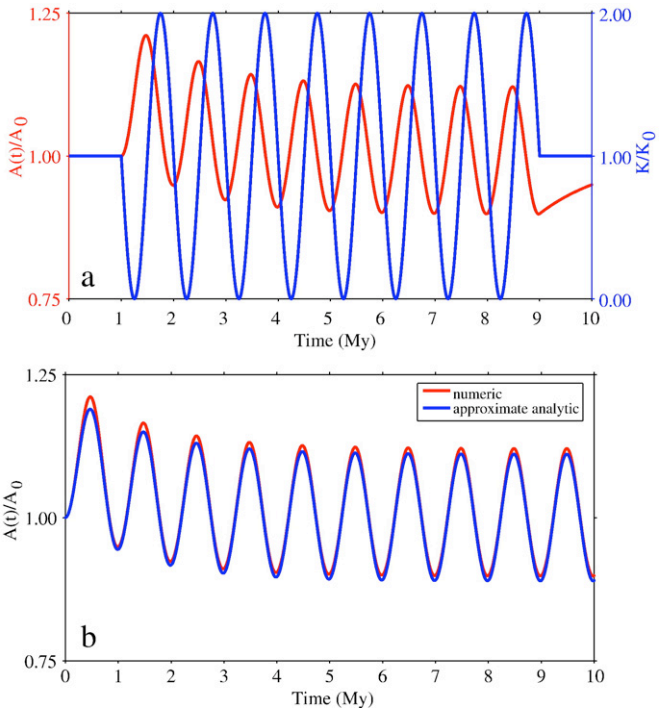

Fig. 3. a) Cross-sectional orogen area (left axis, red), calculated using Eq. (4), that develops as a response to a sinusoidal variation in erosivity K (right axis, blue) around a background erosivity of $K_0=10^{-5}$. The erosivity is modulated harmonically with a 1 million year periodicity, the tectonic influx is constant in time, and the orogen response is measured as the perturbation from the original steady state, A_0. Note that the orogen response is out of phase with the climate forcing by ϕ, which is about 90 degrees in this case. A increases during periods of low erosivity (small K) because more mass is added to the orogen by tectonic accretion than is removed by erosional processes. b) A comparison of orogen cross-sectional area from numerical integration of Eq. (4) and the approximate analytic solution Eq. (8). Here, as in a), $K_0=10^{-5}$, the erosivity is modulated harmonically, the tectonic influx is constant in time, and the orogen response is measured as the perturbation from the original steady state, A_0. The approximate analytic solution underestimates the magnitude of the peak response of the orogen, but does capture 90% of the cross-sectional area evolution including the initial exponential decay.

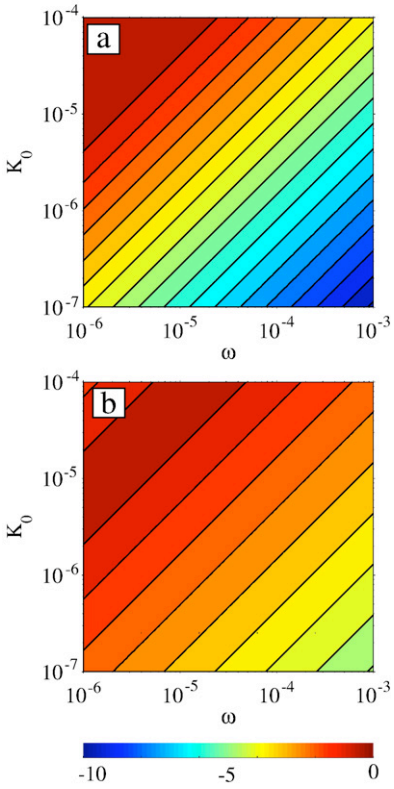

Fig. 4. Variation in perturbed cross-sectional area, A' as a function of erosivity, K_0, and frequency of climate oscillations, ω. Panels a and b show the magnitude of the sine and cosine terms in Eq. (8) Note that the contours are of the base 10 log of the coefficient in Eq. (8). For the range of parameter values $K_0 = 10^{-7}$–10^{-4} yr^{-1}, $\omega = 10^{-3}$–10^{-6} yr^{-1}, the maximum perturbations from the initial cross-sectional area occur when K_0 is relatively large (so that the orogen can respond quickly) and ω is small (long periods) giving the orogen time to evolve.

the local erosion rate (Eq. (5)) thus decreasing the orogen area, and increasing the plate convergence rate. This is the case if precipitation increases on the side of the orogen that overlies the subduction zone interface. Alternatively, if an increase in orogen elevation enhances precipitation on the side of the orogen away from the subduction zone interface, then the coupled side of the orogen may dry out and increase in width, thus decreasing the convergence rate.

Changes to the erosivity may be driven by changes in the local amount of precipitation (Eq. (5)). To understand the effects of gradual changes in climate-modulated erosivity, consider models where the erosivity either increases (from $K = 5\times10^{-7}$ to $K = 5\times10^{-6}$ yr^{-1}) or decreases (from $K = 5\times10^{-6}$ to $K = 5\times10^{-7}$ yr^{-1}) by an order of magnitude (Fig. 2 g, h). As long as the erosivity continues to evolve, a steady state orogen size and convergence rate will not achieve a steady state due to the fact that mass removal rate from the orogen continually varies. Both plate convergence rates and orogen widths can vary by 30–40% as a result of both step-like and gradual climate-modulated changes in erosivity.

Changes in climate state (e.g., precipitation rates) may occur much more rapidly than orogen response time scales. To quantify how sensitive the orogen evolution law is to perturbations of $K = K_0 + K_1$ at different frequencies, we calculate the perturbed response of cross-sectional area $A = A_0 + A_1$. Substituting these perturbed quantities into Eq. (4) with $p = 1$, we obtain,

$$\frac{\mathrm{d}(A_0 + A_1)}{\mathrm{d}t} = Uh - (K_0 + K_1)(A_0 + A_1). \tag{7}$$

We solve for the perturbed cross-sectional orogen area by neglecting higher order terms, noting that $Uh - K_0A_0 = 0$, and assuming that the climate coefficient varies harmonically, $K_1 = K_0 \sin(2\pi\omega t)$. This reduces Eq. (7) to $\mathrm{d}A_1/\mathrm{d}t = -A_0K_0 \sin(2\pi\omega t) - K_0A_1$ which has the solution,

$$\frac{A_1}{A_0} = \frac{K_0\left(2\pi\omega\cos(2\pi\omega t) - K_0\sin(2\pi\omega t) - 2\pi\omega e^{-K_0 t}\right)}{K_0^2 + 4\pi^2\omega^2}. \tag{8}$$

For typical values of K_0 and ω there is a ~90° phase lag between the climate forcing and the orogen response. This is because $\tan^{-1}(-2\pi\omega/K_0)$ is ~90° for $\omega \gg 1$ yr^{-1}, $K_0 \ll 1$ yr^{-1} (Fig. 3a), which is well approximated by Eq. (8) (Fig. 3b). After the initial exponential response, the cross-sectional orogen area perturbation is, $A_1/A_0 < 10^{-3}$ for $K_0 = 10^{-6}$ yr^{-1} and $\omega \approx 10^5$ yr^{-1} (Fig. 4). Thus oscillations in the effective erosivity due to climatic changes at sub-million year time scales do not perturb the mean climate state for a long enough period of time to either enhance or retard the fluvial removal of orogenic material and change the cross-sectional area of the orogen more than 20% (Fig. 4). Thus for the examples described below we consider the evolution of W and U in the presence of relatively slow change in climate state.

4. The Andean orogeny and the evolution of Nazca–South America plate motion

One of the type locales that allows for the application of this theory is the Andean margin at the boundary between the Nazca (NAZ) and South American (SAM) plates. This plate boundary zone margin has been the locus of active deformation, at least as a volcanic arc, since the Jurassic (e.g., James, 1971) and largely convergent plate kinematics have persisted for at least the last 30 Ma (e.g., Pardo-Casas and Molnar, 1987). The combination of pre-existing estimates of convergence rates and paleo-elevations as a function of time makes this an ideal locale in the sense that we have metrics constraining both the convergence rate, U, and the size of the orogen. NAZ–SAM convergence rates over

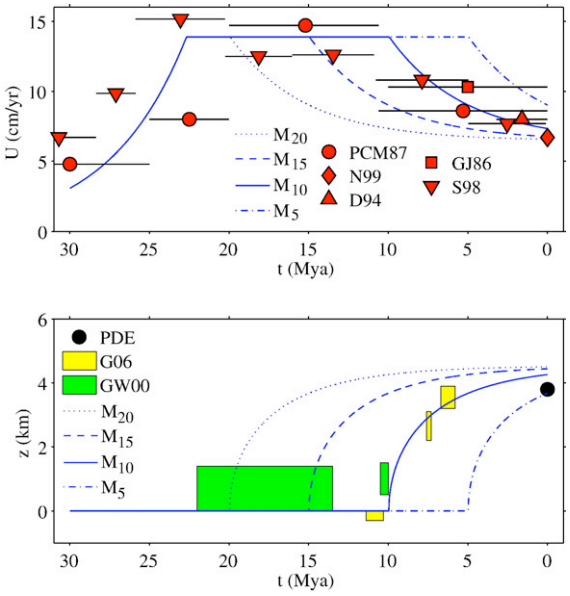

Fig. 5. Upper panel: Nazca–South America plate convergence rates. The five data sets are: 1) Pardo-Casas and Molnar (1987), PCM87; 2) Norabuena et al. (1999), N99; DeMets et al. (1994), D94; Gordon and Jurdy (1986), GJ86; Somoza (1998), S98. Convergence rates increase from a minimum of 5–7 cm/yr at the Oligocene–Miocene boundary to a maximum of ~15 cm/yr between 10 and 25 Ma, then decrease to the present-day value of ~7 cm/yr. Lower panel: Altiplano paleo-elevations. The two sets of observational constraints are an analysis of clumped oxygen isotopes, Ghosh et al., (2006), G06; and a paleo-botanical compilation from Gregory-Wodzicki (2000), GW00. The four models in both panels are for a constant $K = 10^{-7}$ with the initial of orogen growth at 5, 10, 15, and 20 Ma (M_5, M_{10}, M_{15}, and M_{20}, respectively).

the past 30 Ma have been estimated by Pardo-Casas and Molnar (1987) and Somoza (1998) based on sea-floor spreading rates. DeMets et al. (1990) and Gordon and Jurdy (1986) used similar data and plate circuit closure to estimate single interval convergence rates over the past 3 and 10 Ma respectively. Over the past 10 Ma all of these estimates are faster than the present-day convergence rate of 6.7± 0.2 mm/yr constrained by Global Positioning System measurements (Norabuena et al., 1999; Kendrick et al., 2003) (Fig. 5). Convergence rates increase from a minimum of 5–7 cm/yr at the Oligocene–Miocene boundary to a maximum of ~15 cm/yr between 10 and 25 Ma. The exact pattern of the velocity decrease since 10 Ma is somewhat ambiguous, although it has been interpreted as linear in time (e.g., Iaffaldano et al., 2006). In the late Oligocene and early Miocene there is clear evidence for the opposite trend, that is an increase in convergence rates in time from ~5 to ~15 cm/yr (Fig. 5).

In addition to plate convergence rates, important aspects of the vertical evolution of the plate boundary zone, and the size of the Andes, are revealed by estimates of the paleo-elevation of the Bolivian Altiplano between the Eastern and Western Cordillera. Here the average present-day elevation is 3.8 km though the peak elevations of the orogenic wedges on the east and west of the plateau exceed 5 km. It seems unlikely that the altitude of the Altiplano could be greater than that of the bounding orogenic wedges, so we consider Altiplano paleo-elevations as minimum elevation estimates. There are constraints on the paleo-elevation of the Bolivian Altiplano (Fig. 5) from both paleo-botanical (Gregory-Wodzicki, 2000) and oxygen isotope paleo-temperature measurements (Ghosh et al., 2006; Garzione et al., 2006). It should be noted that these estimates have generated significant debate but it appears that the remaining controversy is focused on the interpretation of these measurements rather than the questions regarding possible diagenetic modification of ancient surface paleo-temperature signals (Sempere et al., 2006; Eiler et al., 2006; Hartley et al., 2007; Garzione et al., 2007). The two separate oxygen isotope paleo-thermometer estimates suggest rapid surface uplift from near sea level to ~3.5 km over the time interval from ~10.4 to ~6.8 Ma (Ghosh et al., 2006; Garzione et al., 2006). Elevation estimates based on paleo-botanical proxies are generally complimentary (Gregory-Wodzicki, 2000). Taken as a whole, these paleo-altimetry estimates suggest that the Andes were no higher than 1.4 km between 13 and 22 Ma but may have been as low as sea level at 10 Ma. Assuming a monotonic surface uplift history, the Andes then grew to nearly their present elevation over a period of about 4 Ma starting at 10–11 Ma. Prior to 22 Ma there are no direct paleo-altimetry constraints. If minimum incision estimates derived from Calama Basin records (Rech et al., 2006) are interpreted as a characteristic measure of mass removal near the southeastern margin of the Altiplano, this would imply that elevations may have been as high as 2.0–2.4 km in the earliest Miocene, requiring a non-monotonic surface uplift history for the Andes.

These observations of both convergence rate and surface uplift history can be explained by a coupled orogen-subduction zone model. Prior to 23 Ma NAZ–SAM convergence appears to have accelerated but there are currently no direct paleo-altimetric constraints for this period. Though poorly constrained, the early increase in convergence rate appears to be associated with a period of low to no significant Andean topography. Thus it seems that increases in convergence rate here cannot be explained by a variation in the resisting force of the orogen. Instead, the increase of convergence rate could be driven by the growth of a negatively buoyant subducting slab that is mechanically coherent to depth of ~200 km at 30 Ma. We note that short slabs may form after episodes of slab detachment (e.g. Wortel and Spakman, 2000), although there is no evidence of such an event beneath South America at 30 Ma. In the absence of an orogen to resist subduction, this short slab accelerates due to its increasing negative buoyancy until a steady state velocity of ~15 cm/yr is reached when the slab encounters the 670 km phase transition. With regard to the initial geometry of the slab, there are trade-offs between the initial depth and dip. The results presented thus far are for the $\delta=90°$ case. For more realistic slab dips of 15°–30°, very similar accelerations are predicted with deeper initial slab depths. Given the absence of clear evidence for, or against, a relatively short slab at 30 Ma, and the possibility that mantle dynamics (for example, slab deflection and subsequent penetration of the 670 phase transition (van der Hilst, 1995)) can also induce accelerated flow, we consider the short slab model to be one possible hypothesis that may explain the early Miocene acceleration of Nazca–South America convergence. We focus the rest of the paper on the more recent and better-constrained record of Andean margin evolution.

The approximate temporal coincidence of Andean surface uplift and the deceleration of NAZ–SAM between 10 and 20 Ma (Fig. 5) has been considered as possible evidence of a direct feedback between orogenic growth and plate motions (Garzione et al., 2006; Iaffaldano et al., 2006). To incorporate the effect of a growing orogen, we need to estimate the value of the effective erosion coefficient K_0. Our strategy is to use the linear scaling with respect to precipitation rates (Eq. (5)) to understand how changes in climate state can lead to changes in the effective erosion coefficient. Previous work in Taiwan, where mean annual precipitation can exceed 2 m/yr, has constrained $K_0=1.9\times10^{-5}$ yr^{-1} (Whipple, 2001). Present-day mean annual precipitation in the Calama basin of the Altiplano are at least two orders of magnitude lower (<20 mm/yr, (e.g., Rech et al., 2006)). Thus, relative to Taiwan, Eq. (5) suggests $K_0\sim10^{-7}$ yr^{-1} for the present-day Altiplano. Prior to the mid to late Miocene aridification, mean annual precipitation rates appear to have been an order of magnitude higher (~0.2 m/yr, (Rech et al., 2006)). Thus for the models considered here we analyze the response of the coupled orogen system to variations in the effective erosion coefficient of an order of magnitude ranging from $\sim10^{-6}$ to $\sim10^{-7}$ yr^{-1}.

We consider two classes of models with variable timing for the initiation of Andean growth and compare these to the observations of both NAZ–SAM convergence rate and Altiplano paleo-elevation time histories. The first class of model has no orogen at all until it is artificially allowed to grow at a prescribed time with a fixed erosivity of 10^{-7} yr^{-1} (Fig. 5). The four possible dates that we use for the sudden initiation of orogen growth are 5, 10, 15, and 20 Ma (M_5, M_{10}, M_{15}, M_{20} respectively). The second most recent of these dates (10 Ma) fits both the convergence rate and paleo-elevation data quite well. Earlier dates for the onset of orogenic growth predict a rapid increase in surface elevation before this is actually observed. Also, the 15 and 20 Ma initial models predict convergence rates between 5 and 10 Ma that are slower than estimates from three independent studies (Gordon and Jurdy, 1986; Pardo-Casas and Molnar, 1987; Somoza, 1998). While the predictions of the model with orogen growth starting at 10 Ma account for much of the observed behavior of the Andes, the model is compatible with only the absolute minimum elevation estimates prior to 15 Ma (Gregory-Wodzicki, 2000) and does not suggest a physical mechanism for the sudden triggering orogen growth.

A second class of model (Fig. 6) invokes a time-dependent parameterization of K to initiate orogen growth, which represents the mid to late Miocene change in the mean annual precipitation associated with aridification of the Altiplano and Western Cordillera (e.g., Rech et al., 2006). The four possible dates that we use for the onset of aridification are 5, 10, 15, and 20 Ma (M_5, M_{10}, M_{15}, M_{20} respectively). In all of these cases, the orogen is allowed to develop from an initial condition of no elevation at 30 Ma. At first the orogen growth is limited by a relatively erosive climate (wet) with $K_0=10^{-6}$ yr^{-1} and a relatively slow convergence rate associated with the sinking of the subducting slab to the 670 km phase transition. Once a steady state is reached at ~21 Ma, the orogen has a modest elevation of ~1 km. Notably this prediction is, in general, more consistent with both the paleo-botanically derived elevation estimates that range from 0 to 1.4 km (Gregory-Wodzicki, 2000) and the timing of thermochronologic rock exhumation estimates (e.g. Barnes and Pelletier, 2006), than it is with the case where there is no orogen whatsoever. Decreasing the erosion coefficient at 10 Ma (M_{10}, Fig. 6) provides the best fit to trends of orogen

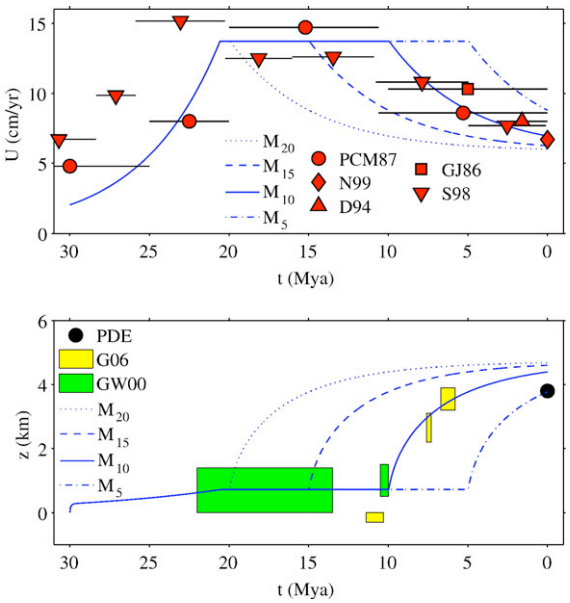

Fig. 6. Same as Fig. 5 but the models include an order of magnitude decrease in erosivity associated with aridification of the western margin of the Andes. Note that for these cases the orogen approaches steady state more slowly and the predicted present-day convergence rates are slower as the less erosive climate allows a larger orogen to grow and slow the descending slab.

growth and plate convergence slowdown, and predicts present-day elevations close to, though above, the observed value of 3.8 km.

Currently, estimates for the onset of aridification of the western Cordillera range from 10 (Hoke et al., 2004) to 25 Ma (Dunai et al., 2005) making the hypothesized link to climatically-driven growth of the Andes somewhat ambiguous. However, coupled atmosphere and ocean models predict that elevation-induced aridification of the western slope scales linearly with elevation up to ~3 km; above this level there are only modest additional elevation effects (Takahashi and Battisti, 2007a,b). Thus, as the Andes increase in elevation, aridification increases, and air parcels are drawn down across the Western Cordillera to the Pacific Ocean, where their relatively low water content enhances evaporative cooling of the local sea surface temperature. Thus, if Andean topography had already grown to 1.4 km by 13 Ma (the maximum bound from paleo-botanical estimates, (Gregory-Wodzicki, 2000) the low lying mountains would induce a cycle of accelerating aridification and orogenic growth, mitigated only by the concomitant deceleration of NAZ–SAM convergence. While this scenario is consistent with the set of observations presented here, it is not explicitly predicted by our models due to the fact that we do not consider the coupled evolution of precipitation above a growing orogenic wedge. Currently, the exact role of maximum and mean topography in the coupled atmospheric circulation and ocean models is not clear (Takahashi and Battisti, 2007b).

An additional mechanism for the surface uplift of the Altiplano is the isostatic response of the upper crust to the detachment of dense eclogitic material from the lowermost crust (Garzione et al., 2006; Molnar and Garzione, 2007). The model presented here does not explicitly require the detachment and removal of lower crustal material in order to rapidly grow the Andes. It instead suggests that a change in the rate of removal of orogenic material allowed for a massive increase in the residence time, and thus elevation, of Andean orogenic material. One of the main arguments for the necessity of the lower crustal detachment hypothesis is that estimated crustal thickening rates are insufficient to uplift the entire surface of the Altiplano over a period of ~4 Ma. It should be noted clearly that our model does not explicitly consider the growth of a plateau but rather assumes that the maximum plateau elevation should scale with the elevation of the orogenic wedge. Thus, in the context of crustal thickening rate arguments, our model would be most consistent with the case where the Altiplano was not raised uniformly but rather the case where what is now recognized as the high plateau grew in width, and thickness, over the last 10 Ma. In fact, Garzione et al. (2006), demonstrated that it would take ~10 Ma to isostatically raise the entire Altiplano by crustal thickening and this is nearly identical to the predictions of our model (Figs. 5 and 6). In the southern Altiplano Elger et al. (2005) have estimated the cessation of significant shortening in the eastern Cordillera at 7–8 Ma. Our model does predict continued post-Miocene shortening, though at a <25% rate between 7 and 10. The suggestion of an isostatic response to the loss of negatively buoyant lower crustal material may be a promising means for generating a small amount of initial elevation that could raise the surface of the Andes from their predicted ~1 km steady state elevation prior to 13 Ma to an excess of 2 km. This increase in surface elevation could trigger a decrease in the local mean annual precipitation, which would lead to rapid orogenic growth.

5. Discussion and conclusions

While we have demonstrated that a coupled orogen-subduction zone model explains the evolution of both orogen elevation and plate convergence rates at the Andean margin, this model may also find applicability in other convergent locales. In particular, it may be interesting to quantify these effects around much of the western and northern boundaries of the Pacific plate, where orogenic wedges including Kamchatka, Japan, and New Zealand have developed in relatively recent times. Such circum-Pacific orogenic changes may be responsible for observed changes in Pacific basin plate motions that have occurred periodically during the Cenozoic and before (e.g., Engebretson et al., 1984; Cande et al., 1995; Wessel and Kroenke, 2007). In fact, many of these observed changes in plate motions, including the one indicated by the change in the Hawaiian–Emperor seamount bend, occur in only a few million years. Such changes occur too rapidly to be explained by changes in plate-driving forces because such forces evolve with mantle buoyancy over time scales of tens of millions of years (e.g., Richards and Lithgow-Bertelloni, 1996). Instead, rapid plate motion changes have previously been attributed to changes in resisting forces acting at plate boundaries, which can evolve over shorter, million year time scales. Although orogenic processes at subduction zones have been previously associated with plate motions changes, it is changes in the dynamics of subduction (e.g., seamount subduction, slab detachment) that typically cause both the coincident plate motion changes and the accompanying orogen response (e.g., Cloos, 1993; Rubin et al., 1995; Jahren et al., 2005). Instead, our model suggests the reverse behavior: changes in orogen size, particularly those caused by climate-induced changes in erosivity, can also be the drivers of rapid changes in plate motions.

While climate-induced changes in erosivity can affect back-arc orogeny and thus subduction rates, changes in the frictional behavior of the plate interface can as well. The effective long term coefficient of friction, μ may vary significantly in subduction zones as a function of sediment (e.g., Ruff, 1989) and water content (e.g., Lamb and Davis, 2003), both of which can change with time in any given location. Recent results from rock mechanics experiments (Di Toro et al., 2004) and numerical integrations of rate and state friction models (e.g., Liu and Rice, 2005) have demonstrated that the coefficient of friction becomes quite small <0.1 at intermediate slip velocities. Thus, the connection between estimates of μ, which are observable on short time scales, and the appropriate parameterization of long term frictional behavior, can be challenging to understand. It is even more difficult to infer how the coefficient of friction may have changed with time in the past because geologic information about plate bounding faults is largely destroyed by the subduction process.

Due to the fact that the orogen gains mass as the plate convergence rate increases, and erodes more quickly as it widens, the coupled model presented here includes a buffering mechanism for the orogen to approach a mass flux steady state. The stabilizing influence of the orogen

in the absence of climatic change may explain the apparently steady 20 mm/yr northward motion of the Arabian plate over the last 50 Ma (McClusky et al., 2000; Chu and Gordon, 1998; Joffe and Garfunkel, 1987). By contrast, the introduction of climatic influences to the same model can lead to relatively rapid changes in plate motion that result from spatially localized orogen growth caused by a new state of erosivity or possibly large-scale river system re-organization (e.g., Clark et al., 2004). To test the hypothesis of climate-change-induced changes in plate motions more broadly will require applying our model in three-dimensions to account for the finite length of an orogen around a plate margin. However, for realistic plate geometries, <50% of the plate margin is directly involved with orogen growth at any given time so that there is a net force exerted on the plate that must be calculated by integrating the force per unit length along the length of the frictional interface. This approach, which has been applied recently to constrain the degree of slab attachment (Conrad et al., 2004) and the bending resistance at subduction zones (Wu et al., 2008), may be particularly interesting for the Pacific plate where the northern and western margins are surrounded by active orogenic systems. Additional important tests of this model will be to compare model predictions not only with plate motion models, paleo-altimetry, and paleo-precipitation rates, but additionally with exhumation rate information that allows us to constrain how quickly rocks have moved through an orogen, and time histories of sediment packages that provide constraints on the rate of mass removal from an orogen (e.g., Clift, 2006). The coupling of our model to a one-dimensional atmospheric model that allows for the calculation of vapor saturation as a function of pressure and temperature (Roe and Baker, 2006) would enable a more direct assessment of how the mean annual precipitation rate is affected by mean and maximum orogen elevation. Four additional effects that have been neglected in this study are partial sediment recycling (e.g., Whipple and Meade, 2004), the hypothesized lubrication effect of subducted sediments (Lamb and Davis, 2003; Sobolev and Babeyko, 2005), the role of dynamically evolving mantle convection (e.g., Wdowinski and O'Connell, 1991), and the role of variable frequency storm intensity (e.g., Snyder et al., 2003).

In summary, the coupled orogen-subduction model described here explains both the late Miocene decrease in NAZ–SAM convergence rate and the simultaneous growth of the Andes as a result of a decrease in the rate of orogen erosion in the Western Cordillera caused by a change to a more arid local climate. The orogen and descending slab are coupled together by the seismogenic frictional interface at the subduction zone. The frictional resistance to subduction increases quadratically with orogenic wedge width and has slowed convergence between the Nazca and South American plates by ~50% over the past 10 Ma. In turn, the rate of orogen growth has decreased and both present-day plate convergence rate and orogen elevations are within 15% of predicted steady state values. Based on the behavior of this system, previous atmospheric modeling, and the range of estimated dates for the onset of high aridity, it is not clear whether widespread dry conditions preceded Andean growth or if the sudden growth of the Andes triggered the arid conditions. Rather, it may have been the case that the Andes were raised relatively slowly at first in an initially relatively erosive (wet) environment but induced a runaway cycle of surface uplift and aridification that was limited only by the decrease in the NAZ–SAM convergence rate associated with increased frictional resistance to subduction. Future observations of paleo-elevation, aridity and increased temporal resolution in plate motions will provide the observational basis for distinguishing between competing geodynamic models and will determine the extent to which climatic changes may modulate plate motions.

Acknowledgements

We thank two anonymous reviewers whose comments helped to improve this manuscript. This project was supported by Harvard University (B.J.M.) and NSF grant EAR-0609590 (C.P.C.).

References

Barnes, J.B., Pelletier, J.D., 2006. Eocene to recent variations in erosion across the central Andean fold-thrust best, northern Bolivia: Implications for plateau evolution. Earth Planet. Sci. Lett. 248, 118–133.
Barr, T.D., Dahlen, F.A., 1988. Thermodynamic efficiency of brittle frictional mountain building. Science 242 (4879), 749–752.
Barr, T.D., Dahlen, F.A., 1989. Brittle frictional mountain building 2. Thermal structure and heat-budget. J. Geophys. Res. Solid Earth Planets 94 (B4), 3923–3947.
Beaumont, C., Jamieson, R.A., Nguyen, M.H., Lee, B., 2001. Himalayan tectonics explained by extrusion of a low-viscosity crustal channel coupled to focused surface denudation. Nature 414 (6865), 738–742.
Bird, P., Kong, X.H., 1994. Computer-simulations of California tectonics confirm very-low strength of major faults. Geol. Soc. Amer. Bull. 106 (2), 159–174.
Buffett, B., 2006. Plate force due to bending at subduction zones. J. Geophys. Res. 111.
Cande, S., Raymond, C., Stock, J., Haxby, W., 1995. Geophysics of the Pitman Fracture Zone and Pacific-Antarctic plate motions during the Cenozoic. Science 270 (5238), 947.
Chapple, W., 1978. Mechanics of thin-skinned fold-and-thrust belts. Bull. Geol. Soc. Am. 89 (8), 1189–1198.
Chu, D., Gordon, R., 1998. Current plate motions across the Red Sea. Geophys. J. Int. 135 (2), 313–328.
Clark, M.K., Schoenbohm, L.M., Royden, L.H., Whipple, K.X., Burchfiel, B.C., Zhang, X., Tang, W., Wang, E., Chen, L., 2004. Surface uplift, tectonics, and erosion of eastern Tibet from large-scale drainage patterns. Tectonics 23 (1).
Clift, P., 2006. Controls on the erosion of Cenozoic Asia and the flux of clastic sediment to the ocean. Earth Planet. Sci. Lett. 241 (3–4), 571–580.
Cloos, M., 1993. Lithospheric buoyancy and collisional orogenesis; subduction of oceanic plateaus, continental margins, island arcs, spreading ridges, and seamounts. Bull. Geol. Soc. Am. 105 (6), 715–737.
Conrad, C.P., Hager, B.H., 1999. Effects of plate bending and fault strength at subduction zones on plate dynamics. J. Geophys. Res. 104 (B8), 17,551–17,571.
Conrad, C.P., Lithgow-Bertelloni, C., 2002. How mantle slabs drive plate tectonics. Science 298 (5591), 207–209.
Conrad, C.P., Bilek, S., Lithgow-Bertelloni, C., 2004. Great earthquakes and slab pull: interaction between seismic coupling and plate–slab coupling. Earth Planet. Sci. Lett. 218 (1–2), 109–122.
Dahlen, F., Suppe, J., 1988. Mechanics, growth, and erosion of mountain belts. Processes in Continental Lithospheric Deformation: Geological Society of America Special Paper, vol. 218, pp. 161–178.
Dahlen, F.A., 1984. Noncohesive critical Coulomb wedges—an exact solution. J. Geophys. Res. 89 (NB12), 125–133.
Dahlen, F.A., Barr, T.D., 1989. Brittle frictional mountain building 1. Deformation and mechanical energy budget. J. Geophys. Res. Solid Earth Planets 94 (B4), 3906–3922.
Davis, D., Suppe, J., Dahlen, F.A., 1983. Mechanics of fold-and-thrust belts and accretionary wedges. J. Geophys. Res. 88 (B2), 1153–1172.
Demets, C., Gordon, R.G., Argus, D.F., Stein, S., 1990. Current plate motions. Geophys. J. Int. 101 (2), 425–478.
DeMets, C., Gordon, R.G., Argus, D.F., Stein, S., 1994. Effect of recent revisions to the geomagnetic reversal time scale on estimates of current plate motions. Geophys. Res. Lett. 21, 2191–2194. doi:10.1029/94GL02118.
Di Toro, G., Goldsby, D.L., Tullis, T.E., 2004. Friction falls towards zero in quartz rock as slip velocity approaches seismic rates. Nature 427, 436–439.
Dunai, T.J., Gonzalez L., G.A., Juez-Larré, J., 2005. Oligocene–Miocene age of aridity in the Atacama Desert revealed by exposure dating of erosion-sensitive landforms. Geology 33 (4), 321–324. doi:10.1130/G21184.1.
Eiler, J., Garzione, C., Ghosh, P., 2006. Response to comment on "Rapid Uplift of the Altiplano Revealed Through 13C-18O Bonds in Paleosol Carbonates". Science 314 (5800), 760c. doi:10.1126/science.1133131.
Elger, K., Oncken, O., Glodny, J., 2005. Plateau-style accumulation of deformation: southern Altiplano. Tectonics 24 (4), TC4020. doi:10.1029/2004TC001,675.
Elsasser, W., 1969. Convection and stress propagation in the upper mantle. The Application of Modern Physics to the Earth and Planetary Interiors, pp. 223–246.
Engebretson, D., Cox, A., Gordon, R., 1984. Relative motions between oceanic plates of the Pacific basin. J. Geophys. Res. 89 (B12), 10,291–10,310.
Forsyth, D., Uyeda, S., 1975. On the relative importance of the driving forces of plate tectonics. Geophys. J. R. Astron. Soc. 43, 163–200.
Garzione, C., Molnar, P., Libarkin, J., MacFadden, B., 2006. Rapid late Miocene rise of the Bolivian Altiplano: evidence for removal of mantle lithosphere. Earth Planet. Sci. Lett. 241 (3–4), 543–556.
Garzione, C.N., Molnar, P., Libarkin, J.C., MacFadden, B., 2007. Reply to comment on "Rapid late Miocene rise of the Andean plateau: evidence for removal of mantle lithosphere" by Garzione et al. (2006) [Earth Planet. Sci. Lett. 241 (2006) 543–556]. Earth Planet. Sci. Lett. 259, 630–633.
Ghosh, P., Garzione, C., Eiler, J., 2006. Rapid uplift of the Altiplano revealed through 13C–18O bonds in Paleosol carbonates. Science 311 (5760), 511–515.
Gordon, R., Jurdy, D., 1986. Cenozoic global plate motions. J. Geophys. Res. 91 (B12), 12,389–12,406.
Gregory-Wodzicki, K., 2000. Uplift history of the Central and Northern Andes: a review. Bull. Geol. Soc. Am. 112 (7), 1091–1105.
Hack, J.T., 1957. Studies of longitudinal stream profiles in Virginia and Maryland. United States Geological Survey Professional Paper, vol. 97 (294-B).
Hartley, A., Sempere, T., Wörner, G., 2007. A comment on "Rapid late Miocene rise of the Bolivian Altiplano: Evidence for removal of mantle lithosphere" by Garzione et al. [Earth Planet. Sci. lett. 241 (2006) 543–556]. Earth Planet. Sci. Lett. 259 (3–4), 625–629.

Hilley, G.E., Strecker, M.R., 2004. Steady state erosion of critical Coulomb wedges with applications to Taiwan and the Himalaya. J. Geophys. Res. 109 (B1). doi:10.1029/2002JB002,284, b01411.
Hoke, G.D., Isacks, B.L., Jordan, T.E., Yu, J.S., 2004. Groundwater-sapping origin for the giant quebradas of northern Chile. Geology 32 (7), 605–608. doi:10.1130/G20601.1.
Husson, L., Conrad, C.P., Faccenna, C., 2008. Tethyan closure, Andean orogeny, and westward drift of the Pacific basin. Earth Planet. Sci. Lett. 271, 303–310.
Iaffaldano, G., Bunge, H., Dixon, T., 2006. Feedback between mountain belt growth and plate convergence. Geology 34 (10), 893–896.
Isacks, B.L., 1988. Uplift of the Central Andean Plateau and bending of the Bolivian Orocline. J. Geophys. Res. 93 (4), 3211–3231.
Jahren, A.H, Conrad, C.P., Arens, N.C., Mora, G., Lithgow-Bertelloni, C., 2005. A plate tectonic mechanism for methane hydrate release along subduction zones. Earth Planet. Sci. Lett. 236 (3–4), 691–704.
James, D., 1971. Plate tectonic model for the evolution of the Central Andes. Bull. Geol. Soc. Am. 82 (12), 3325–3346.
Joffe, S., Garfunkel, Z., 1987. Plate Kinematics of the circum Red Sea; A re-evaluation. Tectonophysics 141, 5–22.
Kendrick, E., Bevis, M., Smalley Jr, R., Brooks, B., Vargas, R., Lauriá, E., Fortes, L., 2003. The Nazca–South America Euler vector and its rate of change. Journal of South American Earth Sciences 16, 125–131.
Kirby, E., Whipple, K., 2001. Quantifying differential rock-uplift rates via stream profile analysis. Geology 29 (5), 415–418.
Lamb, S., Davis, P., 2003. Cenozoic climate change as a possible cause for the rise of the Andes. Nature 425 (6960), 792–797.
Lamb, S., Hoke, L., 1997. Origin of the high plateau in the Central Andes, Bolivia, South America. Tectonics 16, 623–649.
Lave, J., Avouac, J.P., 2001. Fluvial incision and tectonic uplift across the Himalayas of central Nepal. J. Geophys. Res. Solid Earth 106 (B11), 26,561–26,591.
Liu, Y., Rice, J., 2005. Aseismic slip transients emerge spontaneously in 3D rate and state modeling of subduction earthquake sequences. J. Geophys. Res. 110 (B08), 307. doi:10.1029/2004JB003,424.
McClusky, S., et al., 2000. Global Positioning System constraints on plate kinematics and dynamics in the eastern Mediterranean and Caucasus. J. Geophys. Res. Solid Earth 105 (B3), 5695–5719.
McQuarrie, N., 2002. The kinematic history of the central Andean fold-thrust belt, Bolivia; Implications for building a high plateau. Bull. Geol. Soc. Am. 114, 950–963.
Mitrovica, J.X., 1996. Haskell [1935] revisited. J. Geophys. Res. Solid Earth 101 (B1), 555–569.
Molnar, P., Garzione, C., 2007. Bounds on the viscosity coefficient of continental lithosphere from removal of mantle lithosphere beneath the Altiplano and Eastern Cordillera. Tectonics 26 (2).
Norabuena, E., Dixon, T., Stein, S., Harrison, C., 1999. Decelerating Nazca–South America and Nazca–Pacific plate motions. Geophys. Res. Lett. 26 (22), 3405–3408.
Pardo-Casas, F., Molnar, P., 1987. Relative motion of the Nazca (Farallon) and South American plates since Late Cretaceous time. Tectonics 6 (3), 233–248.
Pritchard, M.E., Ji, C., Simons, M., 2006. Distribution of slip from 11 $M_w > 6$ earthquakes in the northern Chile subduction zone. J. Geophys. Res. 111, B10302. doi:10.1029/2005JB004013.
Rech, J.A., Currie, B.S., Michalski, G., Cowan, A.M., 2006. Neogene climate change and uplift in the Atacama Desert, Chile. Geology 34 (9), 761–764. doi:10.1130/G22444.1.
Richards, M., Lithgow-Bertelloni, C., 1996. Plate motion changes, the Hawaiian–Emperor bend, and the apparent success and failure of geodynamic models. Earth Planet. Sci. Lett. 137 (1–4), 19–27.
Roe, G., Baker, M., 2006. Microphysical and geometrical controls on the pattern of orographic precipitation. J. Atmos. Sci. 63 (3), 861–880.
Roe, G., Stolar, D., Willett, S., 2006. Response of a steady-state critical wedge orogen to changes in climate and tectonic forcing. Tectonics, Climate, and Landscape Evolution: Geological Society of America Special Paper, vol. 398 (1).
Rubin, C., Miller, E., Toro, J., 1995. Deformation of the northern Circum-Pacific margin; variations in tectonic style and plate-tectonic implications. Geology 23 (10), 897–900.
Ruff, L.J., 1989. Do trench sediments affect great earthquake occurrence in subduction zones? Pure Appl. Geophys. 129 (1/2), 263–282.
Seidl, M., Dietrich, W., 1992. The problem of channel erosion into bedrock. Catena Supplement 23, 101–124.
Sempere, T., Hartley, A., Roperch, P., 2006. Comment on "Rapid Uplift of the Altiplano Revealed Through 13C–18O Bonds in Paleosol Carbonates". Science 314 (5800), 760. doi:10.1126/science.1132837.
Snyder, N.P., Whipple, K.X., Tucker, G.E., Merritts, D.J., 2003. Importance of a stochastic distribution of floods and erosion thresholds in the bedrock river incision problem. J. Geophys. Res. 108 (B8), 2117.
Sobolev, S., Babeyko, A., 2005. What drives orogeny in the Andes? Geology 33 (8), 617–620.
Somoza, R., 1998. Updated Nazca (Farallon)–South America relative motions during the last 40 My: implications for mountain building in the central Andean region. J. South Am. Earth Sci. 11 (3), 211–215.
Stolar, D., Roe, G., Willett, S., 2007. Controls on the patterns of topography and erosion rate in a critical orogen. J. Geophys. Res. 112.
Suppe, J., 1980. Imbricated structure of western foothills belt, south-central Taiwan. Pet. Geol. Taiwan 17, 1–16.
Takahashi, K., Battisti, D., 2007a. Processes controlling the mean tropical pacific precipitation pattern. Part I: the Andes and the Eastern Pacific ITCZ. J. Climate 20 (14), 3434–3451.
Takahashi, K., Battisti, D., 2007b. Processes controlling the mean tropical pacific precipitation pattern. Part II: The SPCZ and the Southeast Pacific Dry Zone. J. Climate 20 (23), 5696–5706.
van der Hilst, R.D., 1995. Complex morphology of subducted lithosphere into the mantle beneath the Tonga Trench. Nature 374, 154–157.
Vietor, T., Oncken, O., 2005. Controls on the shape and kinematics of the Central Andean plateau flanks: insights from numerical modeling. Earth Planet. Sci. Lett. 236 (3–4), 814–827.
Wdowinski, S., O'Connell, R., 1991. Deformation of the central Andes (15–27 deg S) derived from a flow model of subduction zones. J. Geophys. Res. 96, 12–245.
Wessel, P., Kroenke, L., 2007. Reconciling late Neogene Pacific absolute and relative plate motion changes. Geochem. Geophys. Geosystems 8 (8).
Whipple, K.X., 2001. Fluvial landscape response time: how plausible is steady-state denudation? Am. J. Sci. 301 (4–5), 313–325.
Whipple, K.X., Meade, B.J., 2004. Controls on the strength of coupling among climate, erosion, and deformation in two-sided, frictional orogenic wedges at steady state. J. Geophys. Res. 109, F01011. doi:10.1029/2003JF000019.
Whipple, K.X., Meade, B.J., 2006. Orogen response to changes in climatic and tectonic forcing. Earth Planet. Sci. Lett. 243, 218–228. doi:10.1016/j.epsl.2005.12.022.
Whipple, K.X., Tucker, G.E., 1999. Dynamics of the stream-power river incision model: implications for height limits of mountain ranges, landscape response timescales, and research needs. J. Geophys. Res. Solid Earth 104 (B8), 17,661–17,674.
Willett, S.D., 1999. Orogeny and orography: the effects of erosion on the structure of mountain belts. J. Geophys. Res. Solid Earth 104 (B12), 28,957–28,981.
Wobus, C.W., Hodges, K.V., Whipple, K.X., 2003. Has focused denudation sustained active thrusting at the Himalayan topographic front? Geology 31 (10), 861–864.
Wortel, M., Spakman, W., 2000. Subduction and slab detachment in the Mediterranean–Carpathian region. Science 290 (1910–1917).
Wu, B., Conrad, C.P., Heuret, A., Lithgow-Bertolloni, C., Lallemand, S., 2008. Reconciling strong slab pull and weak plat bending: the plate motion constraint on the strength of mantle slabs. Earth Planet. Sci. Lett. 272, 412–421.